metals

MDPI

Article

Synthesis and Thermoelectric Properties of Ni-Doped ZrCoSb Half-Heusler Compounds

Degang Zhao *, Lin Wang, Lin Bo and Di Wu

School of Materials Science and Engineering, University of Jinan, Jinan 250022, China; mse_wanglin@yeah.net (L.W.); mse_bolin@yeah.net (L.B.); crystal4885@sina.com (D.W.)

* Correspondence: mse_zhaodg@ujn.edu.cn; Tel.: +86-531-8276-7561

Received: 28 December 2017; Accepted: 11 January 2018; Published: 17 January 2018

Abstract: The Ni-doped $ZrCo_{1-x}Ni_xSb$ half-Heusler compounds were prepared by arc-melting and spark plasma sintering technology. X-ray diffraction analysis results showed that all samples were crystallized in a half-Heusler phase. Thermoelectric properties of $ZrCo_{1-x}Ni_xSb$ compounds were measured from room temperature to 850 K. The electrical conductivity and the absolute value of Seebeck coefficient increased with the Ni-doping content increasing due to the Ni substitution at Co. sites. The lattice thermal conductivity of $ZrCo_{1-x}Ni_xSb$ samples was depressed dramatically because of the acoustic phonon scattering and point defect scattering. The figure of merit of $ZrCo_{1-x}Ni_xSb$ compounds was improved due to the decreased thermal conductivity and improved power factor. The maximum ZT value of 0.24 was achieved for $ZrCo_{0.92}Ni_{0.08}Sb$ sample at 850 K.

Keywords: half-Heusler compound; thermoelectric property; ZrCoSb; Ni-doping

1. Introduction

Due to the increasing globe energy demands and dwindling fossil fuel reserves, developing renewable energy conversion technologies is an effective way to solve the energy crisis. Thermoelectric materials show great potential application in the field of waste heat recovery, power generators and solid refrigeration due to their direct conversion between heat energy and electrical energy. The conversion efficiency of thermoelectric material is primarily governed by the dimensionless figure-of-merit, $ZT = \alpha^2\sigma T/(\kappa_L + \kappa_e)\kappa$, where α, σ, $\alpha^2\sigma$, κ_L, κ_e and T are the Seebeck coefficient, electrical conductivity, power factor, lattice thermal conductivity and carrier thermal conductivity of total thermal conductivity κ and absolute temperature, respectively [1–3]. As the physical parameters α, σ, and κ_e are coupled via effective mass (m^*) and carrier concentration (n), it is a major challenge to improve the ZT by independently optimizing these parameters. Normally, there are two approaches to enhance the ZT value. One is the optimization of power factor by band engineering or tuning the carrier concentration and the other is depressing the κ_L by point defect scattering, alloy scattering, nanostructuring et al. [4–6].

Recently, half-Heusler compounds with chemical formula MAB (M = Ti, Zr, Nb, and Hf; A = Co., Ni, and Fe; B = Sn, Sb) and cubic MgAgAs structure (F-43m) have attracted considerable research interest due to their good mechanical strength, non-toxicity and high thermal stability [7–9]. Half-Heusler compounds with 18 valence electron count (VEC) per unit cell have been widely studied as one of the promising thermoelectric materials working in the middle temperature range due to their narrow bandgap and high Seebeck coefficients, such as MCoSb, MNiSn (M = Ti, Zr, Nb, and Hf), et al. [10–14] Among these compounds with 18 VEC, MCoSb based half-Heusler compounds (M = Ti, Zr, Nb, and Hf) have been extensively investigated including the substituting at M, A or B sites and many studies have achieved high thermoelectric properties. Yuan et al. synthesized the $ZrCoSb_{1-x}Sn_x$ by substituting Sn on Sb sites and the maximum ZT value of 0.52 at 973 K was obtained [15]. Hsu et al. demonstrated

that Fe doping can depress the lattice thermal conductivity of $ZrFeCo_{1-x}Sb_x$ and improve the *ZT* [16]. He et al. reported the (Zr, Hf)$Co_{1-x}Ni_xSb$ compounds with a low thermal conductivity were synthesized and the peak *ZT* reached 1.0 at 1073 K [17]. As present, however, most of research about the MCoSb based half-Heusler compounds are *p*-type semiconductor. There are few studies about the *n*-type MCoSb-based half-Heusler compounds.

In this study, the *n*-type Ni-doped $ZrCo_{1-x}Ni_xSb$ half-Heusler alloys were synthesized by arc-melting and spark plasma sintering technology. It is expected that the substitution of Ni on Co. sites can improve the power factor and depress the lattice thermal conductivity. The thermoelectric properties including the electrical transport properties, carrier scattering mechanism and thermal transport properties were discussed.

2. Experimental Procedures

The samples with nominal composition $ZrCo_{1-x}Ni_xSb$ (x = 0, 0.04, 0.08, 0.12) were prepared by arc-melting of Zr (slug, 99.98%), Co (granule, 99.999%), Ni (shot, 99.999%) and Sb (rod, 99.9%) under argon atmosphere. Excess Sb (~5%) was added due to the high vapor pressure of Sb in the process of arc melting. The arc-melted ingots were re-melted three times to ensure compositional homogeneity. Then, the obtained ingots were ground into fine powders in agate mortar. The pulverized powders were consolidated by spark plasma sintering (SPS) process at 1373 K under 60 MPa for 6 min in a vacuum. The density (d) of $ZrCo_{1-x}Ni_xSb$ samples was measured by Archimedes method. X-ray diffraction (XRD, Rigaku Rint 2000, Tokyo, Japan) was used to determine the constituent phase. The microstructure of samples was characterized by a field-emission scanning electron microscopy (FE-SEM, JXA-8200, JEOL, Tokyo, Japan). A ZEM-3 instrument (ULVAC-RIKO, Tokyo, Japan) was used to measure the electrical conductivity and Seebeck coefficient of samples simultaneously in Ar atmosphere. The thermal conductivity of samples was calculated using $\kappa = dC_p\lambda$, where d, C_p, λ are the density, specific heat capacity and thermal diffusivity coefficient. The thermal diffusivity coefficient was measured by a laser flash apparatus (Netzsch, LFA427, Selb, Germany) in a flowing Ar atmosphere. The measurement of specific heat capacity was carried out using a differential scanning calorimetry (Netzsch, DSC404, Selb, Germany). Uncertainty in the electrical conductivity, Seebeck coefficient and thermal conductivity measurements is 3%, 5% and 5%, respectively. The Hall coefficient (R_H) was measured by Van der Pauw's method in vacuum under a magnetic field of $\pm$0.5 T at room temperature. The carrier mobility (μ_H) and carrier concentration (n) were calculated by $\mu_H = R_H\sigma$ and $n = 1/(eR_H)$, where e is the electron charge.

3. Results and Discussion

Figure 1 shows the XRD patterns of the prepared $ZrCo_{1-x}Ni_xSb$ (x = 0, 0.04, 0.08, 0.12) samples. All major diffraction peaks could be indexed to the half-Heusler ZrCoSb phase (JCPDS 54-0448) and no impurity phase is observed, suggesting the Ni-doped $ZrCo_{1-x}Ni_xSb$ half-Heusler alloys are single phase with the same MgAgAs-type crystallographic structure. As the tiny difference of atom radii of Co. and Ni, the lattice parameter of $ZrCo_{1-x}Ni_xSb$ (x = 0, 0.04, 0.08, 0.12) samples was almost equal and no obvious peak shift of XRD was observed. Figure 2 displays the microstructure and the elemental distribution of constituent element of $ZrCo_{0.96}Ni_{0.04}Sb$ half-Heusler sample. It can be clearly seen that all elements were distributed homogeneously and no visible other phase can be found, which is also consistent with the XRD result of Figure 1.

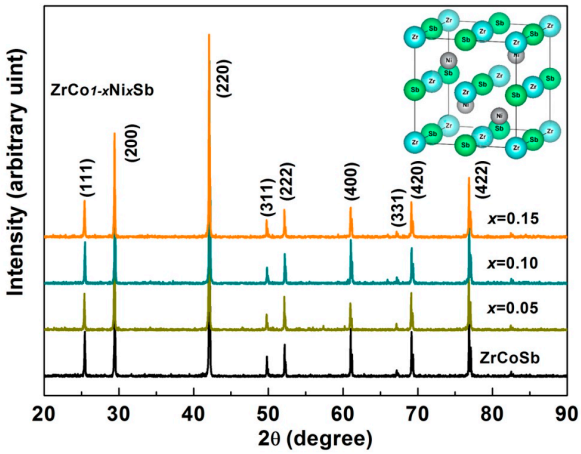

Figure 1. XRD patterns of $ZrCo_{1-x}Ni_xSb$ (x = 0, 0.04, 0.08, 0.12) half-Heusler compounds.

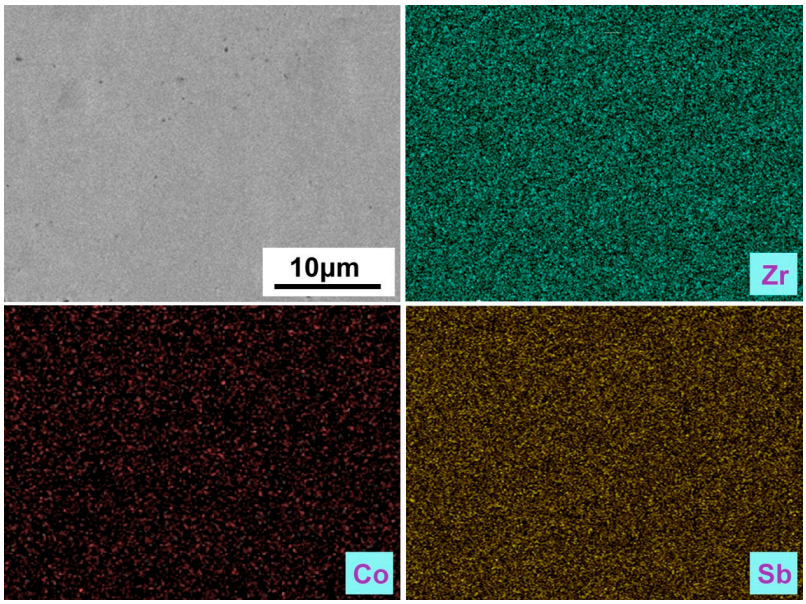

Figure 2. SEM image and elemental maps of $ZrCo_{0.96}Ni_{0.04}Sb$ half-Heusler compound.

Figure 3 presents the electrical properties of $ZrCo_{1-x}Ni_xSb$ half-Heusler samples. The undoped ZrCoSb half-Heusler sample shows a typical semiconducting behavior, and the σ increases with the temperature increasing. The σ of Ni-doped $ZrCo_{1-x}Ni_xSb$ half-Heusler samples is significantly enhanced with the content of Ni increasing. In addition, the σ of Ni-doped $ZrCo_{1-x}Ni_xSb$ samples shows a transition from the semiconducting behavior to semi-metal behavior and the transition temperature shifts to low temperature with the Ni-doping increasing. The enhancement of σ for $ZrCo_{1-x}Ni_xSb$ half-Heusler compounds should be attributed to the increase of carrier concentration (n) and carrier mobility (μ_H), just as shown in Table 1. The n of Ni-doped $ZrCo_{1-x}Ni_xSb$ half-Heusler compounds is in the order of 10^{20} cm^{-3} at room temperature and increases from 1.80×10^{20} cm^{-3} to 5.55×10^{20} cm^{-3} when the Ni-doping content increases from 0 to 0.12. Meanwhile, the measured μ_H increases at room temperature with the Ni-doping concentration increases. For instance, the μ_H increases from 5.08 cm^2/Vs for ZrCoSb to 10.7 cm^2/Vs for $ZrCo_{0.96}Ni_{0.04}Sb$ sample. Figure 3b demonstrates the α of $ZrCo_{1-x}Ni_xSb$ half-Heusler compounds as a function of temperature. The α of all $ZrCo_{1-x}Ni_xSb$ samples is negative, indicating the conductive behavior of $ZrCo_{1-x}Ni_xSb$ half-Heusler compounds is n-type and the major charge carriers are electrons. The absolute value of α of $ZrCo_{1-x}Ni_xSb$ half-Heusler

compounds first increases and then decreases with the Ni-doping concentration increasing. The maximal absolute value of α of $ZrCo_{0.96}Ni_{0.04}Sb$ sample is 63.5 μV/K at 850 K. Moreover, the monotonic increase of α with increasing temperature indicates the single band conduction behavior of $ZrCo_{1-x}Ni_xSb$ half-Heusler compounds. The variation of α may be related to the modification of band structure due to the Ni-doping, which further influences the density of states near the Fermi level. To better understand the dependence of the Seebeck coefficient on the carrier concentration of $ZrCo_{1-x}Ni_xSb$ half-Heusler compounds, Pisarenko plots at 300 K were calculated, just as shown Figure 3c. It is assumed that the single parabolic band (SPB) model and acoustic phonon scattering mechanism are appropriate for the thermoelectric material, Pisarenko plots can be derived based on the relationship between the Seebeck coefficient and DOS effective mass according to the following Formulas (1)–(3) [18,19],

$$\alpha = \pm\frac{k_B}{e}\left[\xi - \frac{(r+5/2)F_{r+3/2}(\xi)}{(r+3/2)F_{r+1/2}(\xi)}\right] \quad (1)$$

$$F_n(\xi) = \int_0^\infty \frac{x^n}{1+e^{x-\xi}}dx \quad (2)$$

$$n = 4\pi\left(\frac{2m^*k_BT}{h^2}\right)^{3/2}F_{1/2}(\xi) \quad (3)$$

where ξ, r, k_B, m^*, and h are the reduced Fermi energy, scattering factor, Boltzmann constant, the density of states effective mass and Planck's constant, respectively. Pisarenko plots is described as

$$\alpha = \frac{8\pi^2k_Bm^*T}{3eh^2}\left(\frac{\pi}{3n}\right)^{2/3} \quad (4)$$

The density of states effective mass of $4.1m_0$ was derived for the Ni-doped $ZrCo_{1-x}Ni_xSb$ half-Heusler compounds, which is higher than that of the undoped ZrCoSb half-Heusler compound ($2.8m_0$). The difference also indicates that the Ni-doping in the $ZrCo_{1-x}Ni_xSb$ half-Heusler plays a beneficial influence on the band structure. Therefore, the α of Ni-doped $ZrCo_{1-x}Ni_xSb$ half-Heusler compounds is improved. In addition, He et al. also reported that the Ni-doping could lead to the large effective mass in the (Hf, Zr)$Co_{1-x}Ni_xSb$ system [17]. The effects of doping on the band structure of ZrCoSb still needs further investigation in the theoretical and experimental aspects. Figure 3d shows the temperature dependence of power factor for $ZrCo_{1-x}Ni_xSb$ half-Heusler compounds. The Ni-doping improves the power factor of $ZrCo_{1-x}Ni_xSb$ half-Heusler compounds evidently. For example, the power factor of $ZrCo_{0.92}Ni_{0.08}Sb$ at 850 K is about 18 $\mu WK^{-2}\cdot cm^{-1}$, which is far higher than that of undoped ZrCoSb sample.

Table 1. Some structural and physical parameters of $ZrCo_{1-x}Ni_xSb$ compounds at room temperature.

x	Relative Density	σ ($\Omega^{-1}\cdot cm^{-1}$)	n (10^{20} cm^{-3})	μ_H (cm^2/Vs)	α (μV/K)	κ_L ($Wm^{-1}\cdot K^{-1}$)	m^* (m_0)
0	98.5%	146	1.80	5.08	−3.4	16.2	2.80
0.04	98.4%	529	4.59	7.20	−74.8	14.2	4.08
0.08	98.8%	773	4.92	9.82	−67.7	12.7	4.09
0.12	98.6%	954	5.55	10.7	−63.5	10.3	4.11

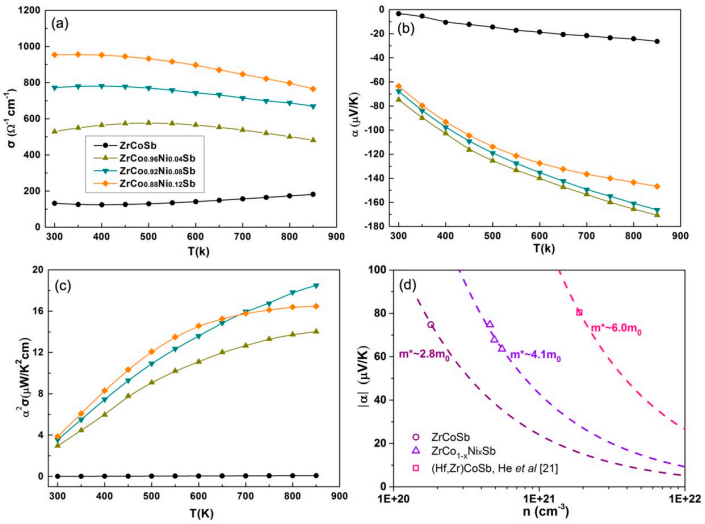

Figure 3. Temperature-dependent electrical properties of $ZrCo_{1-x}Ni_xSb$ half-Heusler samples (**a**) electrical conductivity (**b**) Seebeck coefficient (**c**) power factor (**d**) Pisarenko plots of $ZrCo_{1-x}Ni_xSb$ assuming SPB model.

Figure 4a shows the temperature dependences of κ for $ZrCo_{1-x}Ni_xSb$ half-Heusler compounds. The κ of all samples decreases with the temperature increasing and no bipolar effect occurs, which indicates the acoustic scattering is the dominant process. The κ of $ZrCo_{1-x}Ni_xSb$ half-Heusler compounds decreases with the Ni-doping content increasing. Normally, the κ_L can be obtained by subtracting the κ_e from κ and κ_e can be calculated according to the Wiedemann-Franz law, $\kappa_e = L\sigma T$, where L is the Lorenz constant. Herein, L is calculated using the Formulas (1)–(4) based on the SPB model and acoustic phonon scattering [20], just as shown in Figure 4b.

$$L = \left(\frac{k_B}{e}\right)^2 \left[\frac{(r+7/2)F_{r+5/2}(\xi)}{(r+3/2)F_{r+1/2}(\xi)} - \left(\frac{(r+5/2)F_{r+3/2}(\xi)}{(r+3/2)F_{r+1/2}(\xi)}\right)^2\right] \quad (5)$$

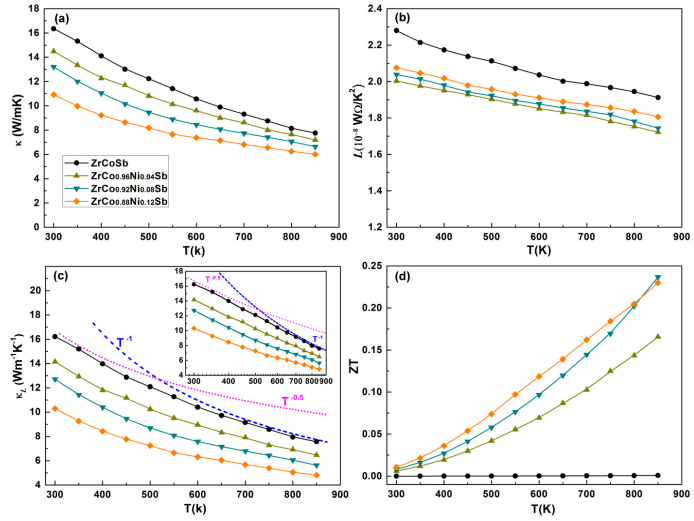

Figure 4. Temperature-dependent (**a**) total thermal conductivity, (**b**) Lorenz constant, (**c**) lattice thermal conductivity, and (**d**) ZT of $ZrCo_{1-x}Ni_xSb$ half-Heusler compounds.

As shown in Figure 4c, the decrease of κ of $ZrCo_{1-x}Ni_xSb$ half-Heusler compounds mainly results from the contribution of κ_L. According to the theory of Klemens-Callaway [21], the substitution of impurity atoms at the host atom site can result in a large number of defect centers due to mass fluctuation (mass differences) and strain field fluctuation (size and interatomic coupling force differences). Therefore, the reduction of κ_L can be attributed to the substitution of Ni at the Co site. Similar results were also found in the TiNiSn, ZrNiSn and TiCoSb systems [22–24]. In addition, the κ_L shows temperature dependence of T^{-1} above 520 K, just as illustrated by blue dot line, indicating that phonon-phonon scattering is the dominant scattering for the Ni-doped $ZrCo_{1-x}Ni_xSb$ half-Heusler compounds in the temperature range from 520 to 850 K. Below 520 K, the κ_L deviates the T^{-1} and follows the $T^{-0.5}$ behavior, suggesting the point defect scattering plays a great role in scattering mechanism. For $ZrCo_{0.88}Ni_{0.12}Sb$ half-Heusler compound, the κ_L is 10.4 W/mK at room temperature which is reduced by 34% than that of undoped ZrCoSb compound and the minimum κ_L of $ZrCo_{0.88}Ni_{0.12}Sb$ is 5.52 W/mK at 850 K. Combined with the electrical and thermal transport properties, the ZT of Ni-doped $ZrCo_{1-x}Ni_xSb$ half-Heusler compounds is calculated and shown in Figure 4d. Due to the reduced κ_L and the enhanced power factor by substituting Ni on Co sites, the ZT value is improved. The highest ZT value of 0.24 is achieved at 850 K for $ZrCo_{0.92}Ni_{0.08}Sb$ half-Heusler compound, which is much higher than that of pristine ZrCoSb half-Heusler compound. As the κ_L of $ZrCo_{1-x}Ni_xSb$ half-Heusler compounds is still high (5~10 W/mK), it is believed that the ZT value may be possibly further improved by appropriate doping or nanostructuring.

4. Conclusions

In this study, the *n*-type Ni-doped $ZrCo_{1-x}Ni_xSb$ half-Heusler compounds were prepared by arc-melting and SPS process. By substituting Ni with Co site, the electrical conductivity of $ZrCo_{1-x}Ni_xSb$ half-Heusler compounds increases due to the great increase in carrier concentration. Meanwhile, the power factor is considerably improved due to the enhanced Seebeck coefficient and electrical conductivity. A maximum power factor of 18 $\mu WK^{-2}\cdot cm^{-1}$ is obtained at 850 K for $ZrCo_{0.92}Ni_{0.08}Sb$ half-Heusler compound. The lattice thermal conductivity of $ZrCo_{1-x}Ni_xSb$ is greatly depressed by Ni substitution and the lowest value of 5.52 W/mK is obtained for $ZrCo_{0.92}Ni_{0.08}Sb$ at 850 K. The ZT value of $ZrCo_{1-x}Ni_xSb$ half-Heusler compound is markedly esnhanced, which is primarily attributed to the increased power factor and the decreased lattice thermal conductivity. The highest ZT value was 0.24 for $ZrCo_{0.92}Ni_{0.08}Sb$ half-Heusler compound at 850 K.

Acknowledgments: Financial supports from the National Natural Science Foundations of China (No. 51772132 and No. 51471076) are gratefully acknowledged.

Author Contributions: All authors participated in the research, analysis and edition of the manuscript. Degang Zhao designed the experiments. Lin Wang and Lin Bo fabricated the samples. Di Wu carried out the measurement of thermoelectric properties. All the authors contributed to the characterization and data analysis. Degang Zhao wrote the paper.

Conflicts of Interest: The authors declare no conflict of interest.

References

1. Ding, L.C.; Akbarzadeh, A.; Tan, L. A review of power generation with thermoelectric system and its alternative with solar ponds. *Renew. Sustain. Energy Rev.* **2018**, *81*, 799–812. [CrossRef]
2. Fitriani, R.O.; Long, B.D.; Barma, M.C.; Riaz, M.; Sabri, M.F.; Said, S.M.; Saidur, R. A review on nanostructures of high temperature thermoelectric materials for waste heat recovery. *Renew. Sustain. Energy Rev.* **2016**, *64*, 635–659. [CrossRef]
3. Cao, Q.M.; Luan, W.L.; Wang, T.C. Performance enhancement of heat pipes assisted thermoelectric generator for automobile exhaust heat recovery. *Appl. Therm. Eng.* **2018**, *130*, 1472–1479. [CrossRef]
4. Champier, D. Thermoelectric generators: A review of applications. *Energy Convers. Manag.* **2017**, *140*, 167–181. [CrossRef]

5. Sajid, M.; Hassan, I.; Rahman, A. An overview of cooling of thermoelectric devices. *Renew. Sustain. Energy Rev.* **2017**, *78*, 15–22. [CrossRef]
6. Liu, W.L.; Hu, J.Z.; Zhang, S.M.; Deng, M.J.; Han, C.G.; Liu, Y. New trends, strategies and opportunities in thermoelectric materials: A perspective. *Mater. Today Phys.* **2017**, *1*, 50–60. [CrossRef]
7. Elghool, A.; Basrawi, F.; Ibrahim, T.K.; Habib, K.; Ibrahim, H.; Idris, D.M. A review on heat sink for thermo-electric power generation: Classifications and parameters affecting performance. *Energy Convers. Manag.* **2017**, *134*, 260–277. [CrossRef]
8. Xue, Q.Y.; Liu, H.J.; Fan, D.D.; Cheng, L.; Zhao, B.Y.; Shi, J. LaPtSb: A half-Heusler compound with high thermoelectric performance. *Phys. Chem. Chem. Phys.* **2016**, *18*, 17912–17916. [CrossRef] [PubMed]
9. Bhattacharya, S.; Madsen, G.K.H. A novel p-type half-Heusler from high-throughput transport and defect calculations. *J. Mater. Chem. C* **2016**, *4*, 11261–11268. [CrossRef]
10. Chauhan, N.S.; Bhardwaj, A.; Senguttuvan, T.D.; Pant, R.P.; Mallik, R.C.; Misra, D.K. A synergistic combination of atomic scale structural engineering and panoscopic approach in p-type zrcosb-based half-Heusler thermoelectric materials for achieving high *ZT*. *J. Mater. Chem. C* **2016**, *4*, 5766–5778. [CrossRef]
11. Fu, C.G.; Zhu, T.J.; Liu, Y.T.; Xie, H.H.; Zhao, X.B. Band engineering of high performance p-type FeNbSb based half-Heusler thermoelectricmaterials for figure of merit $ZT > 1$. *Energy Environ. Sci.* **2015**, *8*, 216–223. [CrossRef]
12. Kangsabanik, J.V.; Alam, A.E. Bismuth based Half Heusler alloys with giant thermoelectric figure of merit. *J. Mater. Chem. A* **2016**, *5*, 6131–6139.
13. Downie, R.A.; Barczak, S.; Smith, R.; Bos, J.W. Compositions and thermoelectric properties of XNiSn (X = Ti, Zr, Hf) half-Heusler alloys. *J. Mater. Chem. C* **2015**, *3*, 10534–10542. [CrossRef]
14. Rausch, E.; Balke, B.; Ouardi, S.; Felser, C. Enhanced thermoelectric performance in the p-type half-Heusler (Ti/Zr/Hf)$CoSb_{0.8}Sn_{0.2}$ system via phase separation. *Phys. Chem. Chem. Phys.* **2014**, *16*, 25258–25262. [CrossRef] [PubMed]
15. Yuan, B.; Wang, B.; Huang, L.; Lei, X.; Zhao, L.; Wang, C. Effects of Sb substitution by Sn on the thermoelectric properties of ZrCoSb. *J. Electron. Mater.* **2016**, *46*, 3076–3083. [CrossRef]
16. Hsu, C.C.; Ma, H.K. Microstructure and thermoelectric properties in Fe-doped ZrCoSb half-Heusler compounds. *Mater. Sci. Eng. B* **2015**, *198*, 80–85. [CrossRef]
17. He, R.; Zhu, H.; Sun, J.; Mao, J.; Reith, H.; Chen, S. Improved thermoelectric performance of n-type half-Heusler $MCo_{1-x}Ni_xSb$ (M = Hf, Zr). *Mater. Today Phys.* **2017**, *1*, 24–30. [CrossRef]
18. Silpawilawan, W.; Kurosaki, K.; Ohishi, Y.; Muta, H.; Yamanaka, S. FeNbSb p-type half-Heusler compound: Beneficial thermomechanical properties and high-temperature stability for thermoelectrics. *J. Mater. Chem. C* **2017**, *5*, 6677–6681. [CrossRef]
19. Rausch, E.; Balke, B.; Stahlhofen, J.M.; Ouardi, S.; Burkhardt, U.; Felser, C. Fine tuning of thermoelectric performance in phase-separated half-Heusler compounds. *J. Mater. Chem. C* **2015**, *3*, 10409–10414. [CrossRef]
20. Romaka, V.V.; Romaka, L.; Rogl, P.; Stadnyk, Y.; Melnychenko, N.; Korzh, R. Peculiarities of thermoelectric half-Heusler phase formation in Zr-Co-Sb ternary system. *J. Alloys Compd.* **2014**, *585*, 448–454. [CrossRef]
21. Schmitt, J.; Gibbs, Z.; Snyder, G.J.; Felser, C. Resolving the true band gap of ZrNiSn half-Heusler thermoelectric materials. *Mater. Horiz.* **2014**, *2*, 68–75. [CrossRef]
22. Huang, L.H.; Zhang, Q.Y.; Wang, Y.M.; He, R.; Shuai, J.; Zhang, J.J. The effect of Sn doping on thermoelectric performance of n-type half-Heusler NbCoSb. *Phys. Chem. Chem. Phys.* **2017**, *134*, 25683–25690. [CrossRef] [PubMed]
23. Downie, R.A.; Maclaren, D.A.; Bos, J.W. Thermoelectric performance of multiphase XNiSn (X = Ti, Zr, Hf) half-Heusler alloys. *J. Mater. Chem. A* **2014**, *2*, 6107–6114. [CrossRef]
24. Liu, Y.F.; Poudeu, P.F. Thermoelectric properties of Ge doped n-type $Ti_xZr_{1-x}NiSn_{0.975}Ge_{0.025}$ half-Heusler alloys. *J. Mater. Chem. A* **2015**, *3*, 12507–12514. [CrossRef]